

Supporting Information

Enhanced molecular alignment in poly-l-lactic acid nanotubes grown via melt-press template wetting

Michael Smith, Cathrin Lindackers, Kevin McCarthy & Sohini Kar-Narayan

1. PLLA nanotubes vs nanowires

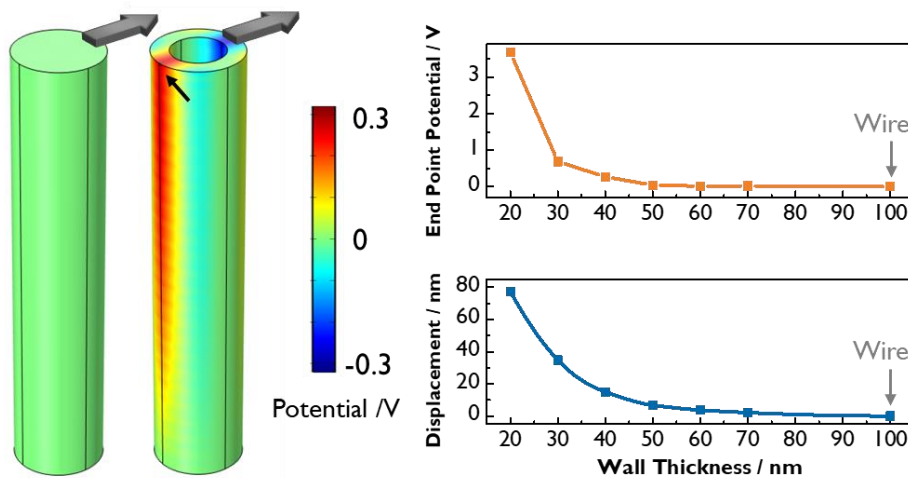


Figure S1. The piezoelectric potential developed as a result of an end load applied to both a solid PLLA nanowire and a hollow nanotube. The potential is maximised in thin walled nanotubes.

Both nanowires and nanotubes can be interesting structures to investigate. In some applications, one geometry is more appropriate than the other. For example, when considering the piezoelectric properties of PLLA, it turns out that a hollow, nanotube structure is optimal is required if a potential is to develop as a result of a bending force, as shown by the simulation data in Figure S1. This finite element modeling was performed using COMSOL Multiphysics 5.2a.

2. Hot stage for melt-press template-wetting

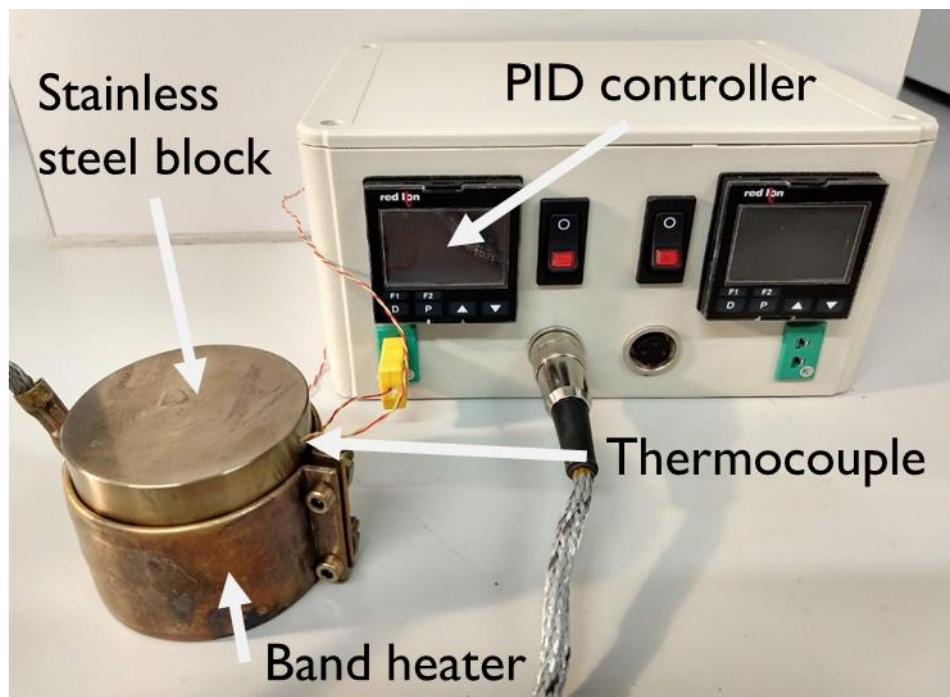


Figure S2. The custom hot stage used for melt-press template-wetting. The second PID controller is currently unused.

3. Nanotube size distribution

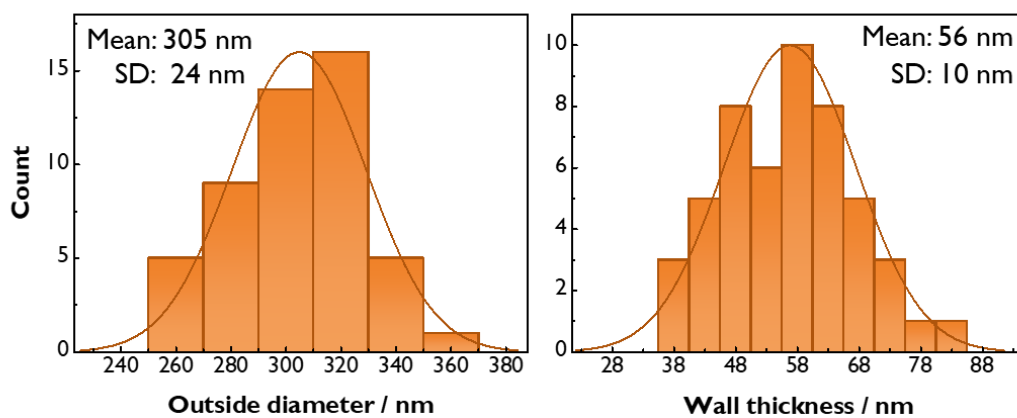


Figure S3. The distribution in outside diameter and wall thickness of PLLA nanotubes grown via melt-press template-wetting. Dimensions were assessed using scanning electron microscopy.

4. Influence of processing parameters

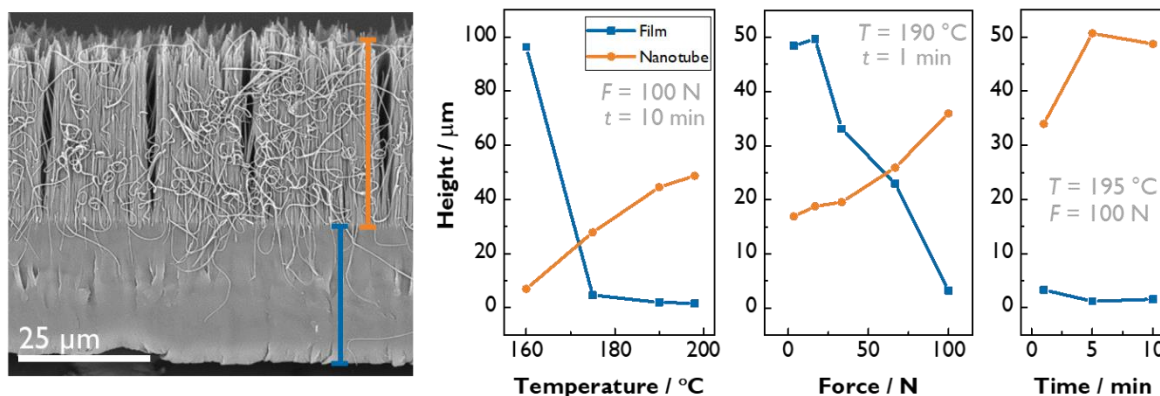


Figure S4. The influence of temperature, force and time on the length of the nanotubes and the thickness of the supporting film beneath.

The thickness of the film is determined solely by the lateral viscous flow of polymer from underneath the template. Higher temperature results in lower viscosity and thus a larger flow rate; greater force generates a faster rate of flow; longer time allows for a greater volume of material to flow from underneath the template.

The length of the nanotubes is dictated by the wetting regimes involved. Given that nanotubes have formed; it is likely that precursor wetting is the dominant growth mechanism. The exact details of this mechanism are not well understood so it is difficult to fully explain the observed trends, however, they are at least consistent with observations reported for polyethylene nanotubes¹. Higher temperatures will change the surface energy of the melt relative to that of the template, thus creating a greater driving force for the spreading of the precursor film. Although the exact mechanism of this spreading is not known², it is reasonable to assume that increased chain mobility at higher temperature also aids in the spreading of the film.

The influence of applied force is interesting, since the wetting of the pores is a result of surface energy considerations rather than physical extrusion. It is possible that applying a higher force simply acts to increase the thermal contact between elements of the system, thus increasing the temperature and consequently nanotube length. The applied force is more important for determining the thickness of the supporting film. The time dependence is in

agreement with the literature - a longer time allows for the precursor film to spread further along the nanopore ¹. The templates used in this work are nominally 60 μm thick, so it is interesting to note that during the time-scales observed here, the nanotubes do not fill the entire length of the pore.

5. Estimating crystallinity from X-ray diffraction data

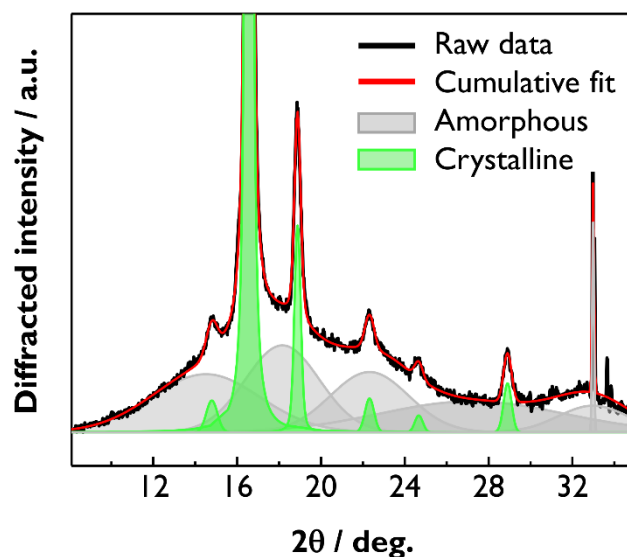


Figure S5 – Fitting peak profiles to XRD data to estimate the amorphous and crystalline scattered intensity. Peak functions are Gaussian, except the main (110)/(200) reflection at $\sim 17^\circ$, which is a Lorentz function.

Crystallinity was estimate for each sample using XRD data. Peak profiles were fitted to the raw data to model the crystalline and amorphous scattered intensity. Fitting was performed using the ‘Fit Peaks’ function within the Peak Analyser Package in Origin 2016. The crystallinty of the samples was determined using the relationship

$$V_c = \frac{I_c}{I_c + KI_a}$$

where V_c is the volume crystalline fraction, I_c and I_a are the total scattered intensities due to the crystalline and amorphous phases, respectively, and K is the relative scattering factor. To facilitate straightforward comparison, a value of $K = 1$ was used. It was assumed that peak area was directly proportional to the scattered intensity. Peak area was determined from numerical integration of the peak profiles over the range $2\theta = [8,35]^\circ$, in line with the minimum and maximum scan angles. Instrumental and thermal broadening were negligible in comparison to the breadth of the peak due to crystallite size.

6. Isothermal DSC heating protocol

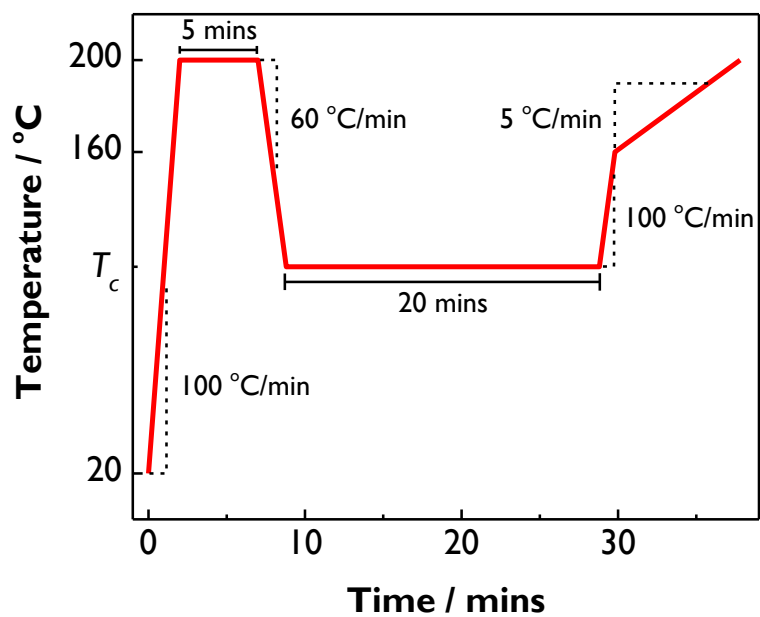


Figure S6. Isothermal DSC experiment protocol. $T_c = 120$ °C for these experiments

7. Conventional Differential Scanning Calorimetry

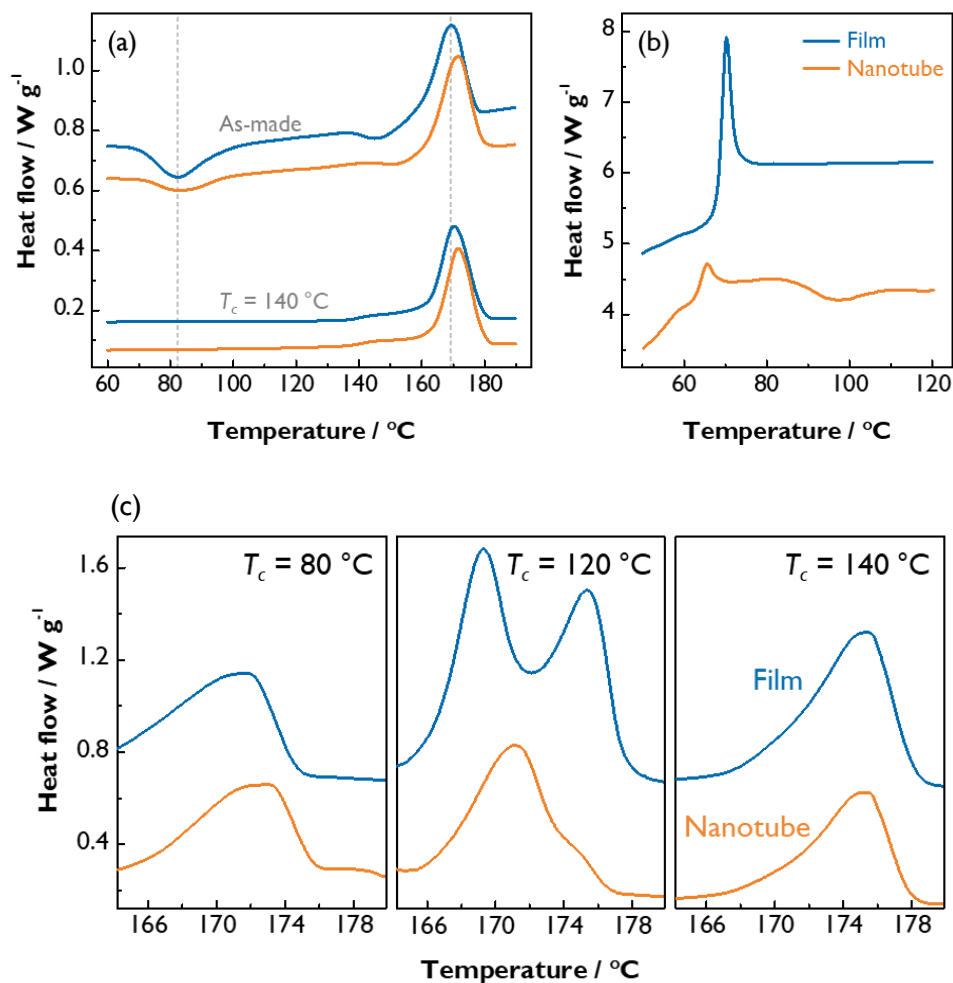


Figure S7. Conventional DSC scans of PLLA film and nanotubes. (a) The Cold crystallisation and melting behaviour of as made and annealed films and nanotubes – heating rate 5 °C/min. (b) The glass transition behaviour of film and nanotubes – heating rate 100 °C/min. (c) The melting point behaviour of film and nanotubes crystallised at different temperatures.

Differential scanning calorimetry (DSC) was used to further investigate the polymer crystalline properties. Typical DSC scans are shown in Figure S6(a) for films and nanotubes, both as-made and after annealing at $T_c = 140$ °C. Significant cold crystallisation events can be seen in both as-made samples, as well as crystal perfection immediately preceding the main melting endotherm. This suggests a significant amorphous component in the as-made samples. Indeed, evaluating the enthalpy associated with the DSC heat flow curves, as outlined by Schawe 3 and Righetti et al. 4 gives crystallinities of -1.6 % and 4 %, respectively, for the film and nanotubes: i.e. amorphous within the experimental error.

The large amorphous content of the as-made samples is also apparent by the presence of glass transition events, as shown in Figure S6(b), for both film and nanotube samples heated at 100 °C/min. This rapid heating is sufficient to suppress cold crystallisation, although a small exotherm can be seen in the nanotube sample.

The melting peak behaviour of nanotube and film samples, annealed at three different temperatures T_c , is shown in Figure S6(c). The double melting peak for films crystallised at $T_c = 120$ °C is indicative of the melt-recrystallisation-melt mechanism associated with the $\alpha' \rightarrow \alpha$ phase transition in PLLA 5–7 . In nanotube samples crystallised at the same temperature, the second melting peak is only visible as a shoulder on the main peak. The more prominent first melting peak suggests a large proportion of the α' phase in the nanotube samples, consistent with the previous observations from WAXD.

8. Calculated Avrami Parameters

Table S1. Calculated Avrami coefficients for PLLA films and melt-press template-wetted nanotubes. Data are presented as mean \pm standard deviation from three separate samples of each

	Film	Nanotube
<i>n</i>	2.09 \pm 0.06	2.069 \pm 0.005
$\tau_{1/2}$ /min	4.78 \pm 0.08	6.08 \pm 0.02

Literature suggests that n for bulk PLLA crystallised at $T_c = 120$ °C typically takes values in the range 2.5 to 3⁸⁻¹¹. The Avrami index of nanoconfined PLLA has not previously been reported, however there is literature regarding similar polymer systems. Computational modelling suggests that the confined environment of a nanopore reduces the Avrami index in comparison to bulk material¹². Experimental data verifies these simulations, with Avrami indices below 2 reported for polyethylene¹³, polypropylene^{14,15} and polyethylene oxide¹⁶ nanowires confined in alumina nanopores.

With this in mind, the Avrami index of 2.096 ± 0.005 calculated for the PLLA nanotubes agrees with the existing literature. Although the outside diameters of the nanotubes are significantly larger than the structures in the above references, it is possible that the nanotube wall is sufficiently thin to retain the nano-confinement effects. However, the inability to produce the expected n value for bulk PLLA in the film samples means that this result cannot currently be trusted. To be conclusive, further investigation, perhaps with samples of greater mass and at different values of T_c , is required.

9. Crystallisation in and out of AAO template

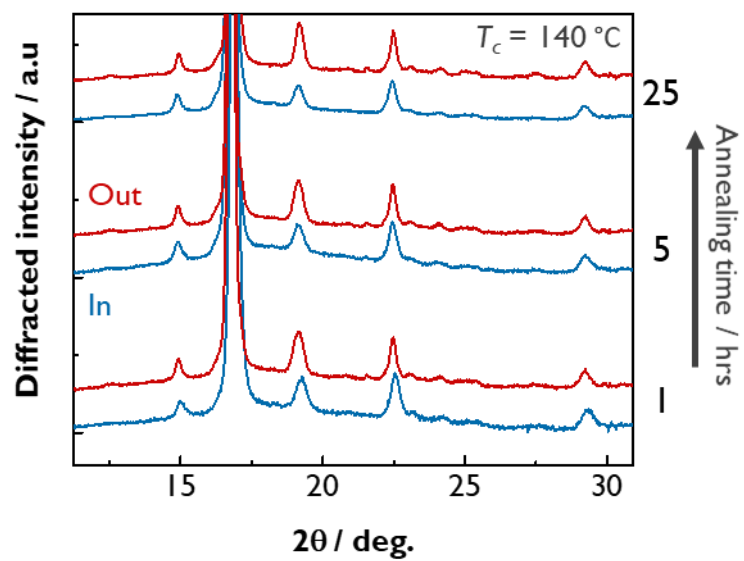


Figure S8. WAXD patterns of PLLA nanotubes annealed 'in' and 'out' of the template material. No significant difference is observed between the two cases, indicating that the pore wall does not have a significant influence on the crystallisation process of PLLA nanotubes.

10. POM with a wave plate

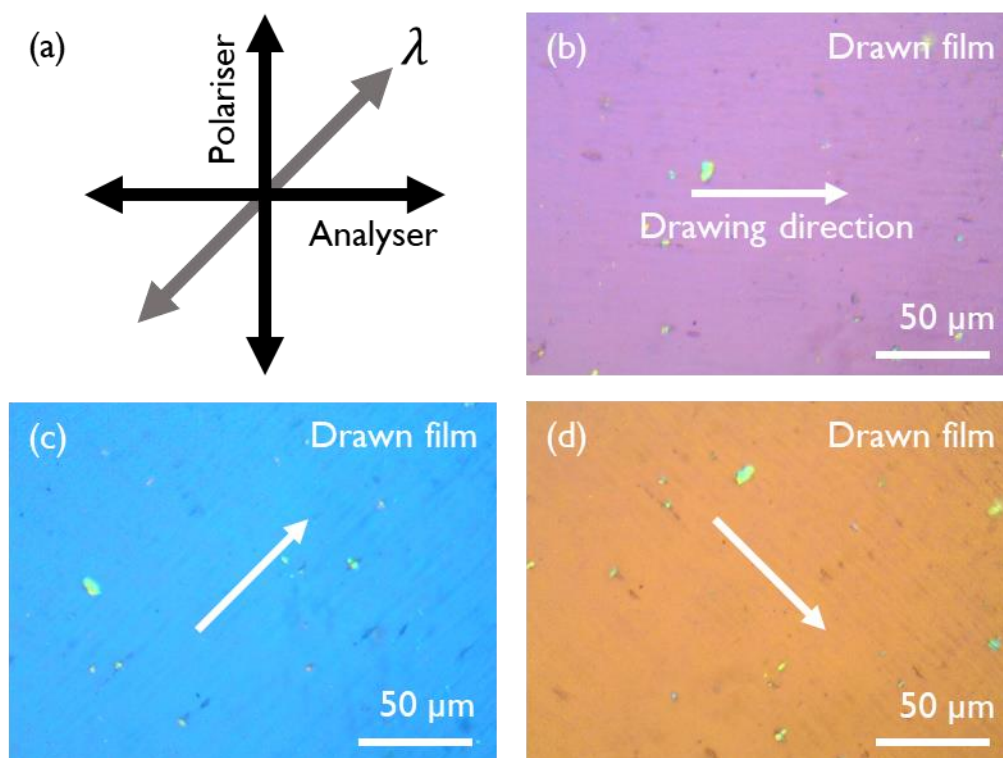


Figure S9. (a) The relative orientation of polariser, analyser and the slow direction of the wave plate used in this investigation, (b) The appearance of a drawn film of PLLA when the drawing direction is neither parallel nor perpendicular to the slow direction of the wave plate (c) The appearance of a drawn film when draw direction and wave plate slow direction are aligned. (d) The appearance of a drawn film when draw direction and wave plate slow direction are perpendicular.

To work out polymer chain orientation from POM, it is necessary to determine the sign of the birefringence of the sample. Determining the sign of birefringence requires the use of a wave plate. A wave plate is a single crystal of a birefringent material cut to a thickness such that, for a given wavelength, the phase difference between fast and slow rays emerging from the plate is an integer multiple of 2π - i.e. a full wavelength of phase difference, hence the name 'wave plate'. When observed between crossed polars, no rotation of the plane of polarisation occurs, and hence this light ray cannot pass through the analyser. This condition is only satisfied for one particular wavelength, so if the wave plate is illuminated with white light, only this specific wavelength will be removed from the spectrum by the analyser. Most wave plates are cut such that green light ($\lambda = 540 \text{ nm}$) is extinguished, thus a wave plate appears magenta (white light minus green) when illuminated with white light through crossed polars.

The orientations of the fast and slow directions of the wave plate are known. Typically the slow direction is marked on the plate itself and set at 45° in a clockwise sense to the vertical of the field of view. Aligning the polariser direction with the vertical then ensures that the wave plate itself is not in extinction relative to the polariser or analyser.

The birefringent sample of interest can then be added to the beam path, so that the the birefringent properties of the wave plate and sample are superimposed. If the slow direction of the sample aligns with the slow direction of the wave plate, the total birefringence is increased. The polarisation of green light is now rotated slightly more than 2π and hence can pass through the analyser. Instead, red light emerges from the sample with a full wavelength of phase difference and is consequently removed by the analyser. The sample therefore appears cyan (white light minus red).

Conversely, if the fast direction of the sample is aligned with the slow direction of the wave plate, the total birefringence is decreased. Blue light is removed by the analyser and the sample appears yellow. By inspecting the colours of the sample as a function of its orientation relative to the slow direction of the wave plate, the fast and slow directions of the sample can be determined.

Drawn polymers are excellent reference samples for POM as they are macroscopically anisotropic and give unambiguous information about the direction of the chain alignment.

When used as a reference in POM, the drawing direction of the polymer sample is aligned with the slow axis of the wave plate, therefore also aligning the polymer chains parallel to the slow axis of the wave plate. By observing the colour of the sample in this orientation, the designations of the slow and fast directions relative to the polymer chain axis can be determined. This information can then be used to interpret the colours seen in a sample of the same polymer for which the chain orientation is unknown. The combination of POM with a

wave plate and a drawn polymer reference sample is therefore an exceptionally useful tool to determine polymer chain orientation.

References

- (1) Yung, K. L.; Kong, J.; Xu, Y. Studies on Flow Behaviors of Polymer Melts in Nanochannels by Wetting Actions. *Polymer (Guildf)*. **2007**, *48* (26), 7645–7652.
- (2) Steinhart, M.; Wehrspohn, R. B.; Gösele, U.; Wendorff, J. H. Nanotubes by Template Wetting: A Modular Assembly System. *Angew. Chemie Int. Ed.* **2004**, *43* (11), 1334–1344.
- (3) Schawe, J. E. K. Remarks Regarding the Determination of the Initial Crystallinity by Temperature Modulated DSC. *Thermochim. Acta* **2017**, *657* (August), 151–155.
- (4) Righetti, M. C.; Gazzano, M.; Di Lorenzo, M. L.; Androsch, R. Enthalpy of Melting of α' - and α -Crystals of Poly(l-Lactic Acid). *Eur. Polym. J.* **2015**, *70*, 215–220.
- (5) Yasuniwa, M.; Iura, K.; Dan, Y. Melting Behavior of Poly(l-Lactic Acid): Effects of Crystallization Temperature and Time. *Polymer (Guildf)*. **2007**, *48* (18), 5398–5407.
- (6) Di Lorenzo, M. L. Calorimetric Analysis of the Multiple Melting Behavior of Poly(L-Lactic Acid). *J. Appl. Polym. Sci.* **2006**, *100* (4), 3145–3151.
- (7) Androsch, R.; Schick, C.; Di Lorenzo, M. L. Melting of Conformationally Disordered Crystals (α' -Phase) of Poly(l-Lactic Acid). *Macromol. Chem. Phys.* **2014**, *215* (11), 1134–1139.
- (8) Kolstad, J. J. Crystallization Kinetics of Poly(L-Lactide-Co-Meso-Lactide). *J. Appl. Polym. Sci.* **1996**, *62* (7), 1079–1091.
- (9) Zhou, W. Y.; Duan, B.; Wang, M.; Cheung, W. L. Crystallization Kinetics of Poly(L-Lactide)/Carbonated Hydroxyapatite Nanocomposite Microspheres. *J. Appl. Polym. Sci.* **2009**, *113* (6), 4100–4115.
- (10) Tsuji, H.; Takai, H.; Saha, S. K. Isothermal and Non-Isothermal Crystallization Behavior of Poly(l-Lactic Acid): Effects of Stereocomplex as Nucleating Agent. *Polymer (Guildf)*. **2006**, *47* (11), 3826–3837.
- (11) Iannace, S.; Nicolais, L. Isothermal Crystallization and Chain Mobility of Poly (L -Lactide). *J. Appl. Polym. Sci.* **1997**, *64* (5), 911–919.
- (12) Ma, Y.; Hu, W.; Hobbs, J.; Reiter, G. Understanding Crystal Orientation in Quasi-One-Dimensional Polymer Systems. *Soft Matter* **2008**, *4* (3), 540.
- (13) Woo, E.; Huh, J.; Jeong, Y. G.; Shin, K. From Homogeneous to Heterogeneous Nucleation of Chain Molecules under Nanoscopic Cylindrical Confinement. *Phys. Rev. Lett.* **2007**, *98* (13), 1–4.
- (14) Li, L.; Liu, J.; Qin, L.; Zhang, C.; Sha, Y.; Jiang, J.; Wang, X.; Chen, W.; Xue, G.; Zhou, D. Crystallization Kinetics of Syndiotactic Polypropylene Confined in Nanoporous Alumina. *Polym. (United Kingdom)* **2017**, *110*, 273–283.
- (15) Duran, H.; Steinhart, M.; Butt, H. J.; Floudas, G. From Heterogeneous to Homogeneous Nucleation of Isotactic Poly(Propylene) Confined to Nanoporous Alumina. *Nano Lett.* **2011**, *11* (4), 1671–1675.
- (16) Michell, R. M.; Blaszczyk-Lezak, I.; Mijangos, C.; Müller, A. J. Confinement Effects on Polymer Crystallization: From Droplets to Alumina Nanopores. *Polym. (United Kingdom)* **2013**, *54* (16), 4059–4077.